ATMOSPHERIC LASER AND INFRARED TRANSMISSION MODEL

REPORT PA702T2

David A. Lee
Robert V. Hemm, Jr.

LMI
GOVERNMENT CONSULTING

JANUARY 2009

NOTICE:

THE VIEWS, OPINIONS, AND FINDINGS CONTAINED IN THIS REPORT ARE THOSE OF LMI AND SHOULD NOT BE CONSTRUED AS AN OFFICIAL AGENCY POSITION, POLICY, OR DECISION, UNLESS SO DESIGNATED BY OTHER OFFICIAL DOCUMENTATION.

Contents

Figures

Tables

Chapter 1
Introduction

This report describes the 2008 version of the Atmospheric Laser and Infrared Transmission (ALIRT) model developed by LMI for the Tactical Air Division of the Office of the Secretary of Defense, Program Analysis and Evaluation. ALIRT is a physical optics model that implements a method for calculating the peak[1] and average fluence delivered to an airborne or ground-based target from a laser weapon on an airborne platform, when the beam propagates through the inhomogeneous, absorbing, scattering atmosphere (refraction and extinction), which is in turbulent motion (turbulence), and when heating of the air by the beam (blooming) may have significant effects. The purpose of the ALIRT model is to support analysis of the use of high-energy lasers and infrared equipment in air combat engagement and campaign analyses.

ALIRT models both 1.3152 micron (μ) and 1.060μ wavelength lasers. There is continuing interest in the potential for use of airborne, tactical, high energy laser weapons. Early efforts in this area focused on 10.6μ wavelength carbon dioxide (CO2) and 3.8 μ wavelength deuterium fluoride (DF) chemical lasers. Current interest is focused on 1.3152 μ chemical oxygen iodine (COIL), and electrically-powered solid state lasers. The most mature high energy solid state laser technology is flashlamp-pumped 1.06 μ neodymium/glass (Nd:glass), however, diode pumping, and alternative lasing molecules and substrates are under active consideration.

ALIRT user inputs include laser power, telescope diameter, laser platform altitude and speed, target bearing, range and relative speed, target incidence angle, and a choice of atmospheres. Outputs include target height from a spherical earth; diffraction-limited, turbulence-scattered, absorbed, and thermally bloomed intensity plots; and numerical intensity data. For modeling simplicity, we maintain separate ALIRT models for 1.3152 μ wavelength iodine and 1.060 μ wavelength neodymium/glass lasers.

In Chapter 2, we describe ALIRT's Microsoft Excel spreadsheet and Visual Basic (VB) structure. Chapter 3 is an ALIRT user guide. The appendix details the calculations of peak fluence and target interaction.

[1] Here, the term "peak" refers to the maximum of the ensemble average fluence. Peak does not refer to the short-term spot peak fluence. Turbulence causes movement of the beam, which can manifest itself either as smearing (if the movement is small relative to the short-term beam diameter) or by hopping around (if the movement is large relative to the short-term beam diameter).

Chapter 2
ALIRT Model Structure and Flow

ALIRT is implemented in an Excel workbook containing several spreadsheets, and the model includes both spreadsheet and VB calculations. This chapter describes the spreadsheets, VB subroutines, and model flow. In a major revision from earlier versions, we have moved many large-array calculations from the spreadsheets into VB, significantly increasing execution speed.

ALIRT Spreadsheet Structure

ALIRT includes a primary user input/output spreadsheet—"Main"—plus spreadsheets for data, calculations, and intermediate results. The spreadsheets also include calculations of final outcome data that are linked to the "Main" user input/output spreadsheet. Table 2-1 lists and briefly describes the ALIRT spreadsheets.

Table 2-1. ALIRT Spreadsheets

Name	Description
Main	Primary program control and user input/output display
test	Intermediate plot data output and plots
wind	Cross-beam wind calculation
fulltraj	Parallel calculations of turbulence effects for checks
cn2	Comparison of Cn^2 models
SR	Unused—early turbulence calculations
blooming	Blooming
xtn	Calculation of extinction for 0 to 15 km altitude
abs	Calculation of molecular and aerosol absorption for 0 to 15 km altitude
att1315_1	1976 Standard Atmosphere molecular and aerosol absorption data
att1315_1_m	1976 Standard Atmosphere molecular extinction data
att1315_2	PcLnWin Mid-latitude Summer molecular and aerosol absorption data
att1315_2_m	PcLnWin Mid-latitude Summer molecular extinction data
att1315_3	PcLnWin Mid-latitude Winter molecular and aerosol absorption data
att1315_3_m	PcLnWin Mid-latitude Winter molecular extinction data

Please note that the generic spreadsheet name "att1315_" is used for both 1.3 μ and 1.06 μ data.

ALIRT VISUAL BASIC STRUCTURE

Primary Subroutines

Four buttons on the “Main” spreadsheet control the VB code in ALIRT. Three buttons control selection of the modeling atmosphere. The current three options are 1976 Standard Atmosphere, PcLnWin Mid-latitude Summer, and PcLnWin Mid-latitude Winter. Adding atmospheres would be straightforward. The fourth button, “Geom,” initiates a run of the main program, by calling the subroutine “runplots.” Runplots calls the subroutines shown in Table 2-2.

Table 2-2. Primary Subroutines Called by Subroutine Runplots

Subroutine	Description
init	Retrieves input parameters for laser height, target range, and target bearing.
slickray	Computes refracted ray from laser to target by integrating the beam equations, starting with the user-input weapon height and look angle, filling the arrays x(i) and h(i) that give distance along the refracted ray and altitude of points on the ray.
integral	Approximates the turbulence integral $\int_{z=0}^{1} C_n^2(h(zR)(1-z)^{\frac{5}{3}}dz$ numerically using the trapezoidal rule. The subroutine assumes x(i) and h(i) are in place, from slickray. Results are placed in global variable “integ “for use by other routines.
plotfreespace	Plots the intensity in kilowatts/cm^2 of the TEM00 Gaussian beam propagating in free space, and the same quantity for that beam propagating through turbulence and impacted by atmospheric extinction and thermal blooming, at normal incidence on the target. The subroutine uses the value of integ, produced by subroutine “integral.” Extinction and blooming data are taken from sheets “xtn” and “bloom,” respectively. Peak axis intensity values for a beam affected by diffraction, by turbulence, by extinction, and by blooming striking a target at normal incidence are output to “Main.” Plot contour values for these intensities and for blooming are output to “test” and plotted, and the plot is copied to “Main.”
plotcontours	Plots three contours of constant intensity, for a TEM00 beam affected by turbulence, extinction, and blooming incident at a user-specified incident angle on a plane surface. The contours are output to “test,” and the plot is copied to “Main.” The peak intensity value is output to “Main.” The peak intensity for the bloomed beam at normal incidence is output to “Main” from “plotcontours.” The subroutine assumes public variables wturb and paxisturb have been evaluated by subroutine plotfreespace.

Primary Functions

In addition to the subroutine structure, ALIRT uses several VB functions in the calculations. Table 2-3 lists and describes them.

Table 2-3. Primary Functions Used by ALIRT

Function	Description
stda_ndx	Refractive index of 1976 Standard Atmosphere
nmwl_ndx	Refractive index of Mid-latitude Winter Atmosphere
xmls_ndx	Refractive index of Mid-latitude Summer Atmosphere
dstda_ndx	Derivative of Standard Atmosphere refractive index
dnmwl_ndx	Derivative of Mid-latitude Winter refractive index
dxmls_ndx	Derivative of Mid-latitude Summer refractive index
Huff_vall57	Huffnagel-Valley model of C_n^2
clear1	Clear I night model of C_n^2

ALIRT CALCULATION FLOW

On “Main” spreadsheet, the user chooses an atmosphere option and enters laser power and mirror diameter. The user specifies the engagement geometry, giving the weapon height, the range to the target, the target’s bearing and elevation, and the angle of inclination of the laser beam on the target surface. It is important to note that the target elevation angle and range inputs are the elevation and range of the refracted ray seen at the laser; they are not the elevation angle or the range of the straight line to the target.

The user also inputs the platform’s airspeed and the target’s velocity relative to the platform. Relative velocity inputs are coordinates of target velocity in a rectangular Cartesian reference frame moving with the weapon aircraft, which is assumed to be in straight, level, unaccelerated flight. The “axial,” “crossing,” and “vertical” axes coincide, respectively, with the weapon aircraft’s roll, pitch, and yaw axes. All axes are positive away from the aircraft.

When all inputs are made, the user clicks “Geom,” which invokes a sequence of VB subroutines and spreadsheet calculations. The first of these is a calculation of the refracted ray’s path through the inhomogeneous atmosphere. This is done by numerical integration of the ray equation, following a method of Roland Berton.[1] We neglect earth’s oblateness and assume that refractive index is a function of height only. We do not consider earth-grazing effects.

[1] Roland P.H. Berton, “Variational Calculation of Three-Dimensional Atmospheric Refraction: Part I, Description and Validation of the Method,” *Journal of Optics A: Pure and Applied Optics,* August 2006, pp. 817–830.

We use the refracted ray rather than a straight line in space for two reasons. First, refractive effects can cause noticeable variations in the turbulence parameter C_n^2 even though they cause only small departures from the straight line, because C_n^2 varies strongly with height at certain altitudes. Second, we want to be consistent with Ontar Corporation's PcLnWin calculations, which use refracted paths.

With the refracted ray path computed, ALIRT calculates the diffraction-limited intensity pattern at the target. We use the standard paraxial approximation for free-space propagation of a TEM00 Gaussian beam, which results in a Gaussian beam on the target.[2] We realize that the assumption of a TEM00 beam is a heavy one, in view of the many features of real lasers that militate against such a simple beam. Nevertheless, we make that assumption, deferring introduction of more complex beam models until we have data on the beam structures of specific laser weapons.

Next, ALIRT evaluates the impact of atmospheric turbulence on the beam. The calculations of turbulence effects use methods given in *The Infrared Handbook*.[3] The calculations involve an integral along the center axis of the refracted beam, which ALIRT approximates by the trapezoidal rule. The end result is a prediction for ensemble averages of the turbulence-impacted beam intensity on the target as Gaussian, with a larger diameter than that of the free-space TEM00 beam.

ALIRT then evaluates the effects of atmospheric extinction. We do this by developing the atmospheric extinction coefficient as a function of height above a spherical earth and then integrating along the refracted beam axis. In essence, the atmospheric extinction function is an interpolation in tabular data for the logarithm of the extinction coefficient, which we obtain from Ontar's PcLnWin application package.[4] The tabular data from PcLnWin are contained in spreadsheets att1315_1, att1315_1m, att1315_2, att1315_2m, att1315_3, and att1315_3m. The index 1 indicates PcLnWin data for the 1976 Standard Atmosphere, index 2 denotes data for Mid-latitude Winter, and index 3 indicates data for Mid-latitude Summer. The index m denotes molecular absorption data, used in blooming calculations. We assume that extinction attenuates the beam without distorting the shape of the ensemble-averaged intensity variation.

Finally, ALIRT models the impact of blooming. The calculations follow the method of Weichel, as given in the American Physical Society's report on boost-phase intercept systems for national missile defense.[5] Energy input for

[2] The calculations are described in LMI, *2007 Atmospheric Laser and Infrared Tracking Model: Some Considerations for Interactions of High-Power Laser Beams with Targets*, Report PA603T3, David A. Lee, September 2007; relevant portions are in the appendix to this document.

[3] See Note 2.

[4] The modeling of the atmospheric extinction coefficient is detailed in LMI Report PA603T3, relevant portions of which are in the appendix to this document.

[5] American Physical Society, *Report of the American Physical Society on Boost-Phase Intercept Systems for National Missile Defense*, July 2003.

blooming is taken to be molecular absorption, obtained from PcLnWin and provided in spreadsheets att1315_xm, where x is 1, 2, or 3, as explained above.[6]

Our models have certain limitations. We neglect earth's oblateness and do not consider earth-grazing effects on propagation. Our model of atmospheric extinction extends only to 15 km height. ALIRT was originally developed to study laser weapons for tactical air-to-air engagements, for which the 15 km limit is adequate.

A box on the "Main" spreadsheet shows the beam's minimum altitude; the user is thus warned if grazing might be a problem. The beam's maximum altitude also is displayed. ALIRT may be used for cases involving greater heights, but the user should note that the results will be those for which atmospheric extinction disappears at altitudes above 15 km.

[6] Further details on the blooming calculations are given in the appendix.

Chapter 3
ALIRT User Guide

All ALIRT operations use the "Main" spreadsheet. Figure 3-1 shows the spreadsheet's control buttons, input numbers, and output numbers, and Figures 3-2 and 3-3 show the output plots.

Figure 3-1. "Main" Spreadsheet: Control Buttons, Input Numbers, and Output Numbers

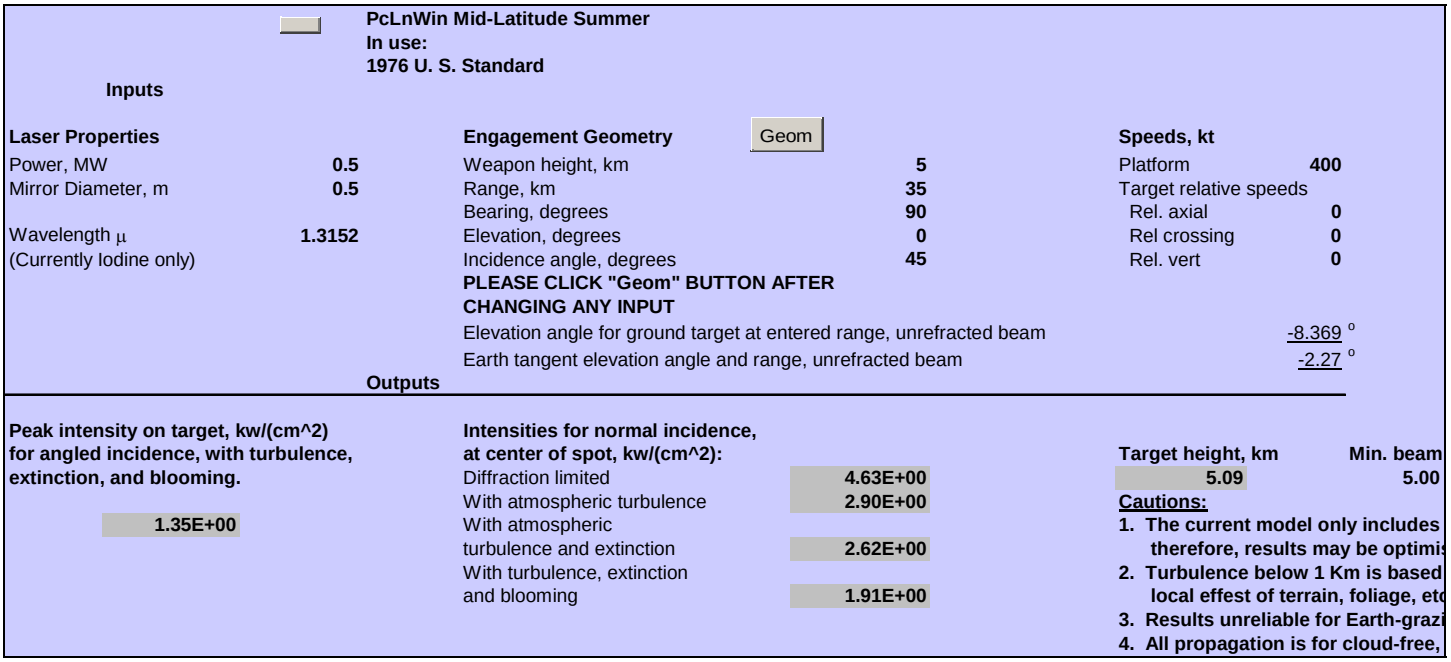

Figure 3-2. "Main" Spreadsheet: Normal Incidence Intensity Profile Plots

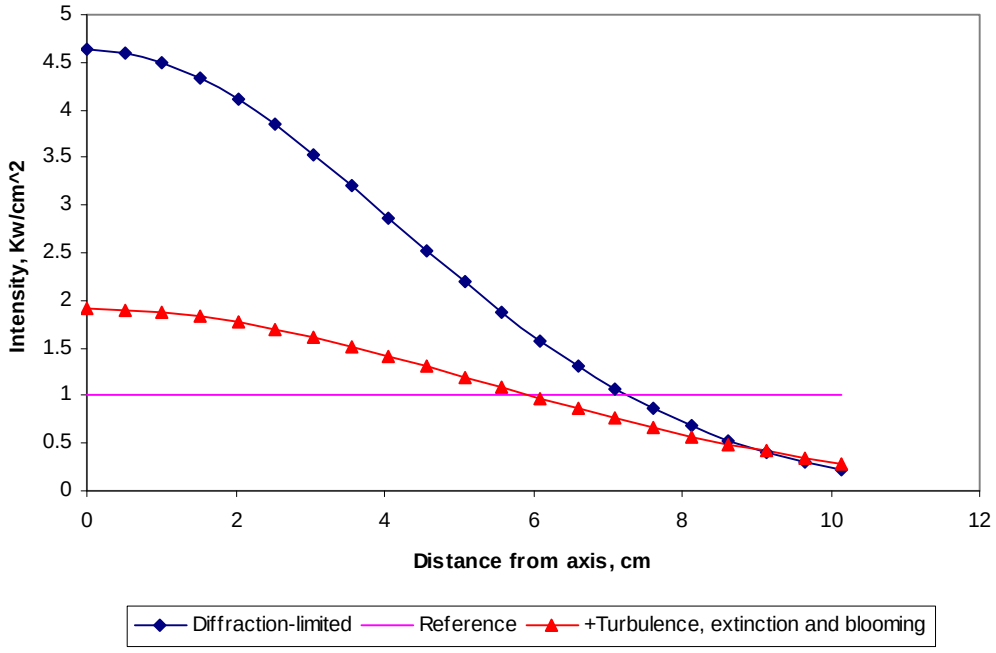

Figure 3-3. "Main" Spreadsheet: Selected Incidence Angle Spot Size Plots

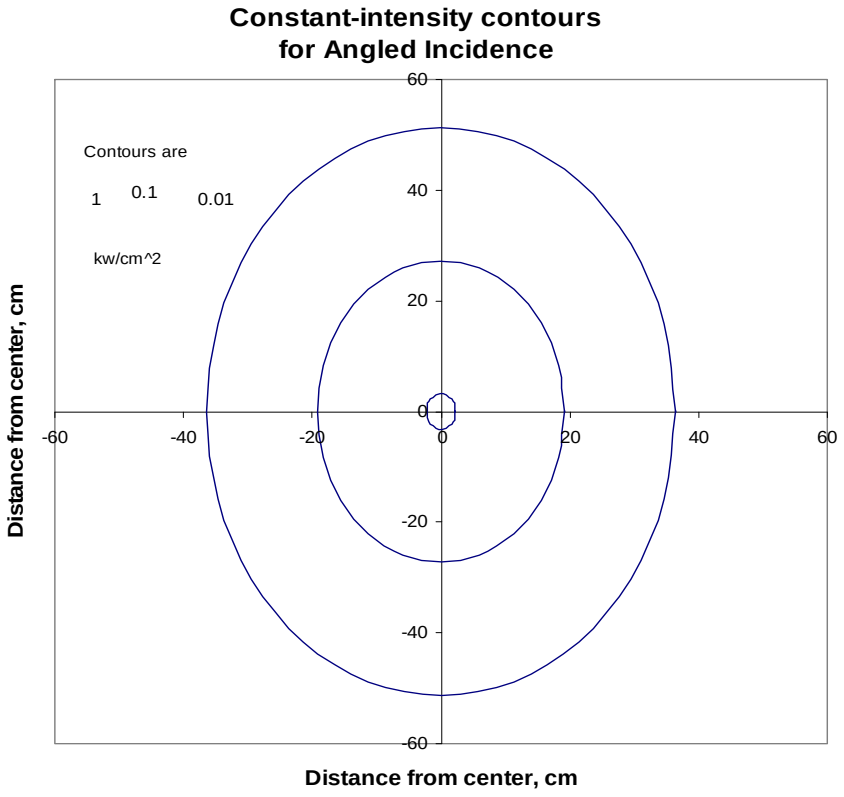

Using ALIRT requires the following actions:

1. Set atmosphere by clicking the button beside the desired atmosphere. ALIRT posts the name of the chosen atmosphere.

2. Enter laser power in megawatts and mirror diameter in meters.

3. Enter weapon height and range in kilometers.

4. Enter target bearing in degrees. Bearing is the angle between the weapon aircraft's flight direction and the line of sight to the target, which is assumed to be to port.

5. Enter target elevation in degrees. Elevation is the angle between the refracted laser ray to the target as it leaves the weapon aircraft and the plane as determined by the aircraft's roll and pitch axes.

6. Enter the angle of incidence of the laser ray on the target. Perpendicular incidence is 0 degree. ALIRT's calculations do not treat grazing effects, so the incidence angle should not be greater than 60 degrees in magnitude.

7. Enter the weapon aircraft's true airspeed in knots.

8. Enter the components of the target aircraft's velocity relative to the weapon aircraft, in knots: "axial" component is in the direction of the weapon aircraft's roll axis, "crossing" component is in the direction of the weapon aircraft's pitch axis, and "vertical" component is in the direction of the weapon aircraft's yaw axis.

When these entries are complete, click "Geom." ALIRT then posts these outputs:

1. Plots of intensity vs. radial distance from the center of the beam for the diffraction-limited beam and for the beam affected by turbulence, extinction, and blooming.

2. Intensities at the center of the beam at normal incidence on the target, in kw/cm^2, for the diffraction-limited beam; for the beam affected by diffraction and turbulence; for the beam affected by diffraction, turbulence, and extinction; and for the beam affected by diffraction, turbulence, extinction, and blooming.

3. Target height and minimum height of the refracted beam. The minimum height can be less than either weapon height or target height for ranges greater than the earth-grazing distance.

4. The elevation angle of the straight line from the weapon to a ground target. The elevation angle of the refracted beam striking a ground target will be slightly greater (algebraically) than this value. For the data shown in

Figure 3-1, the earth-strike elevation of the refracted ray is −5.855 degrees, rather than the −5.873-degree elevation of the straight line.

5. The elevation angle and length of the straight line from the weapon that is tangent to the earth. This information is intended to help the user avoid grazing beams, which ALIRT's calculations do not treat.

Appendix
Calculations of Peak Fluence and Target Interaction

This appendix consolidates and updates material from LMI reports [1] and [2]. Certain sections describe significant improvements in the model.

The appendix begins with a brief overview. We then derive the field equations we use, starting with Maxwell's equations and identifying our assumptions. Next, we develop an integral equation for electromagnetic propagation in a random medium occupying a half-space, with field values prescribed on the bounding plane. The integral equation allows us to describe diffraction effects and to address the effects of imperfect initial beam quality. It also serves as our starting point for turbulence, extinction, blooming, and other calculations. A mathematical note at end of the appendix develops expressions for the electric field and for intensity (power density).

MODELING OVERVIEW

ALIRT treats the effects of beam quality, diffraction, atmospheric turbulence, atmospheric absorption and scattering, and blooming on the energy delivered at not-necessarily-normal incidence on a not-necessarily-plane target.

We do not consider improvements by adaptive optics for two reasons. First, we expect the tactical engagements of interest to take place at ranges of no more than a few tens of kilometers, reducing the impacts of atmospheric turbulence significantly in comparison with those of strategic laser weapon engagements expected to occur at ranges of some hundreds of kilometers. Second, we want to see what might be done with tactical laser weapons without the complexity, weight, initial cost, and maintenance expense associated with adaptive optics.

The extensive literature on Gaussian beams treated with the classical Rytov model of turbulence-induced fluctuations in refractive index allows us to describe the combined effects of diffraction and turbulence.

We developed models of extinction coefficient and molecular absorption from PcLnWin outputs in Ontar [3]. We used these models to calculate effects of atmospheric extinction and blooming.

Much of the material in this appendix is available in standard references, particularly Andrews and Phillips [4] and the references cited in that work. For our discussions of beam quality and of non-normal incidence, we need certain

details of Gaussian beam propagation. For completeness and clarity, we derive the results that we need. This makes our notation conventions clear (no wondering if wave number is the reciprocal of wavelength or 2π times that value) and explicitly identifies the important assumptions.

THE FIELD EQUATIONS

In a medium with constant permeability μ_0 and variable, scalar permittivity ε, and no true currents or true charges, Maxwell's equations are

$$\begin{aligned} \nabla \cdot (\varepsilon \vec{E}) &= 0 \\ \nabla \cdot \vec{H} &= 0 \\ \nabla \times \vec{E} &= -\mu_0 \frac{\partial \vec{H}}{\partial t} \\ \nabla \times \vec{H} &= \frac{\partial (\varepsilon \vec{E})}{\partial t} \end{aligned} \qquad \text{[Eq. A-1]}$$

As is usual in beam propagation analyses, we assume that spatial gradients and time derivatives of ε are negligibly small compared with those of the field components. We also set

$$\vec{U}(x_1, x_2, z, t) = \vec{U}(x_1, x_2, z) e^{-i\omega t} \qquad \text{[Eq. A-2]}$$

where $\vec{U}$ is either of $\vec{E}$ or $\vec{H}$.

With those assumptions, Equations A-1 imply that both electric and magnetic fields are solenoidal and that

$$\nabla \times \vec{E} = i\omega\mu_0 \vec{H} \qquad \text{[Eq. A-3]}$$

and

$$\nabla \times \vec{H} = -i\omega\varepsilon \vec{E}\,. \qquad \text{[Eq. A-4]}$$

Taking the curl of Equation A-3, using the fourth of Equations A-1 to express the curl of $\vec{H}$ in terms of $\vec{E}$, and recalling that the curl of the curl of a solenoidal vector field is the negative of the Laplacian of the field, we find that the electric field satisfies

$$\nabla^2 \vec{E} + \omega^2 \mu_0 \varepsilon \vec{E} = 0 \qquad \text{[Eq. A-5]}$$

at interior points of the medium.

Introducing a spatially varying electric susceptibility χ, we find

$$\nabla^2\vec{E} + \omega^2\mu_0\varepsilon_0(1+\chi)\vec{E} = 0 \qquad \text{[Eq. A-6]}$$

or

$$\nabla^2\vec{E} + k^2(1+\chi)\vec{E} = 0 \qquad \text{[Eq. A-7]}$$

where

$$k^2 \equiv \omega^2\mu_0\varepsilon_0 = \frac{\omega^2}{c_0^2} \qquad \text{[Eq. A-8]}$$

and c_0 is the speed of light in free space.

AN INTEGRAL EQUATION FOR A FIELD COORDINATE

We are interested in electric field coordinates $U(x_1,x_2,z)$ that satisfy Equation A-7 in the half-space $z > 0$, with the boundary condition

$$U(x_1, x_2, 0) = U_0(x_1, x_2), \qquad \text{[Eq. A-9]}$$

where $U_0(x_1, x_2)$ is a prescribed boundary value function, and a radiation condition specifying that energy propagated by the electromagnetic field moves toward increasing values of z for sufficiently large z. Such a field coordinate will satisfy the equation

$$\nabla^2 U + k^2 U = -k^2\chi U \qquad \text{[Eq. A-10]}$$

and the boundary condition Equation A-9.

The boundary value problem posed by Equation A-9 and the equation

$$\nabla^2 U + k^2 U = f(x_1, x_2, z) \qquad \text{[Eq. A-11]}$$

may be solved with a Green's function $G(\vec{x},\vec{y})$ that has the following conditions:

1. $\nabla_y^2 G + k^2 G = 0$ in R^+, where R^+ denotes the half-space $y_3 > 0$ with the point $\vec{y} = \vec{x}$ excluded; here ∇_y^2 denotes the Laplacian operator applied to the components of $\vec{y}$.

2. $G(\vec{x},\vec{y}) = \dfrac{e^{ik|\vec{x}-\vec{y}|}}{|\vec{x}-\vec{y}|} + o(|\vec{x}-\vec{y}|^{-1})$ as $|\vec{x}-\vec{y}| \downarrow 0, \forall\, \vec{x}$ with $x_3 > 0$.

3. $G(\vec{x},\vec{y}) \equiv 0$, when $y_3 = 0$.

When such a function can be found, the solution of the boundary value problem posed by Equation A-9 and Equation A-11 may be written as

$$4\pi U(\vec{x}) = \iiint_{R^+} G(\vec{x},\vec{y}) f(\vec{y}) dv_y - \iint_{y_3=0} \frac{\partial G(\vec{x},\vec{y})}{\partial y_3} U_0(y_1,y_2) dy_1 dy_2 . \quad \text{[Eq. A-12]}$$

It is not difficult to show that the function

$$G(\vec{x},\vec{y}) = \frac{e^{ik|\vec{x}-\vec{y}|}}{|\vec{x}-\vec{y}|} - \frac{e^{ik|\vec{x}-\vec{y}_-|}}{|\vec{x}-\vec{y}_-|} \quad \text{[Eq. A-13]}$$

satisfies conditions 1, 2, and 3, where $\vec{y}_- \equiv (y_1, y_2, -y_3)$. Consequently, a field component U that satisfies Equation A-9 and Equation A-10 satisfies the integral equation

$$4\pi U(\vec{x}) = -k^2 \iiint_{R^+} G(\vec{x},\vec{y}) \chi(\vec{y}) U(\vec{y}) dv_y - \iint_{y_3=0} \frac{\partial G(\vec{x},\vec{y})}{\partial y_3} U_0(y_1,y_2) dy_1 dy_2 . \quad \text{[Eq. A-14]}$$

DIFFRACTION AND BEAM QUALITY

We will study diffraction and beam quality with Equation A-14, specialized to the case $\chi \equiv 0$. In this case, Equation A-14 gives

$$U(\vec{x}) = -\frac{1}{4\pi} \int_{-\infty}^{\infty} \int_{-\infty}^{\infty} \frac{\partial G(\vec{x},\vec{y})}{\partial y_3} U_0(y_1,y_2)\, dy_1 dy_2 . \quad \text{[Eq. A-15]}$$

Differentiating the function $G(\vec{x},\vec{y})$ of Equation A-13 with respect to y_3 gives

$$\left.\frac{\partial G(\vec{x},\vec{y})}{\partial y_3}\right|_{y_{3=0}} = -2\left(\frac{ik}{r_0} - \frac{1}{r_0^2}\right)\frac{x_3}{r_0} e^{ikr_0} \quad \text{[Eq. A-16]}$$

where

$$r_0 \equiv \sqrt{(x_1-y_1)^2 + (x_2-y_2)^2 + x_3^2} . \quad \text{[Eq. A-17]}$$

We are interested in the beam far from the initial plane $x_3 = 0$. We assume that the beam's intensity is negligible except inside a right circular cone of angle Ψ, whose axis is the x_3 axis and where Ψ does not exceed a few tens of microradians.

(The following analytic results can be checked for consistency with this assumption, and observations support its relevance to actual beams.)

With this assumption, for all values of x_1, y_1 of interest,

$$\frac{(x_1 - y_1)^2 + (x_2 - y_2)^2}{x_3^2} << 1. \qquad \text{[Eq. A-18]}$$

Using this assumption, writing r_0 as

$$r_0 = x_3\sqrt{1 + \frac{(x_1 - y_1)^2 + (x_2 - y_2)^2}{x_3^2}}\,, \qquad \text{[Eq. A-19]}$$

expanding the radical in powers of $\frac{(x_1 - y_1)^2 + (x_2 - y_2)^2}{x_3^2}$, retaining the leading term in the denominators of Equation A-16, and retaining the two leading terms in the exponential function of that equation,[1] we find

$$\left.\frac{\partial G(\vec{x},\vec{y})}{\partial y_3}\right|_{y_{3=0}} = -\frac{2ik}{x_3}\exp\left[\frac{ik}{x_3} + \frac{ik}{2x_3}\left[(x_1 - y_1)^2 + (x_2 - y_2)^2\right]\right] \qquad \text{[Eq. A-20]}$$

so that

$$U(\vec{x}) = -\frac{ik}{2\pi x_3}e^{ikx_3}\int_{-\infty}^{\infty}\int_{-\infty}^{\infty}\exp\left[\frac{ik}{2x_3}\left[(x_1 - y_1)^2 + (x_2 - y_2)^2\right]\right]U_0(y_1, y_2)\,dy_1 dy_2\,. \qquad \text{[Eq. A-21]}$$

Equation A-21 gives values of the field coordinate $U(\vec{x})$ far from the initial plane and allows us to consider the effects of beam quality and diffraction.

Effects of Beam Quality

Under certain conditions on $U_0(x_1, x_2)$, which we state below, the propagating field will have relatively simple characteristics, such as those of the TEM_{00} mode. But some features of high-power lasers militate against this. In a transverse-flow gas laser, upstream depletion of the inversion may destroy axial symmetry of the output. Support structures for optics may block parts of the output beam. Vibrating structures (jitter) may spoil intended symmetries or distort the beam.

[1] The additional term is kept in the exponent because $kx_3\tan\Psi$ may be large compared with 1, and so affect phase in the beam, while $kx_3(\tan\Psi)^4$ will be small compared with 1. For example, if the beam is negligible for distances greater than 1 meter from its axis at a range of 20 km, so that Ψ = 50 μradian, when λ = 1.3 μ, $kx_3\tan\Psi = O(10^6)$, while $kx_3(\tan\Psi)^4 = o(10^{-7})$.

To develop some understanding of departures from TEM_{00}, we suppose that $U(\vec{x})$ is the coordinate of a rectilinearly polarized electric field, and that

$$U_0(x_1,x_2)=\frac{1}{W_0}\sum\sum e^{i\phi_{mn}}\sqrt{\frac{P_{mn}R_0}{2^{m+n-2}\pi m!n!}}H_m(\frac{\sqrt{2}x_1}{W_0})H_n(\frac{\sqrt{2}x_2}{W_0})\exp\left[-\left(\frac{1}{W_0^2}+\frac{ik}{2F_0}\right)r^2\right] \quad \text{[Eq. A-22]}$$

where the sums range over a set of values of m and n, where $r^2=x_1^2+x_2^2$, where $R_0\equiv\sqrt{\frac{\mu_0}{\varepsilon_0}}$ = 377 Ω is the "resistance of free space," and where ϕ_{mn} is a phase factor chosen, with P_{mn}, to make the sum represent the initial field. The H_j are Hermite polynomials of order j.

This is not the most general expression for the field boundary values—the widths in the x_1 and x_2 directions need not be equal—but, by virtue of the completeness property of Hermite polynomials, it is capable of representing a reasonably diverse class of initial fields. The components of the sum may be called "components" of the input field.

Equation A-22 represents an initial field that has been modified by reflection in a thin parabolic mirror with focal length F_0. By virtue of the orthogonality property of the Hermite polynomials, the total power P in the input is the sum of the powers P_{mn} of the individual components.

For the rectilinearly polarized electric field that we are considering, the Poynting vector will point along the x_3-axis, and the magnetic field, like the electric field, will be perpendicular to that axis. It is customary to speak of the component with indices m, n as a "Gauss-Hermite $TEM_{m,n}$ mode."

In the mathematical note at the end of this appendix, we develop expressions for the electric field and for intensity (power density) at distances x_3 from the initial plane, for the Gauss-Hermite $TEM_{m.n}$ mode. In the focal plane $x_3 = F_0$, the field is

$$U(x_1,x_2,F_0)=\frac{-i}{W}\sum\sum e^{i\phi_{mn}}i^{m+n}\sqrt{\frac{P_{mn}R_0}{2^{m+n-2}\pi m!n!}}H_m(\frac{\sqrt{2}x_1}{W})H_n(\frac{\sqrt{2}x_2}{W})\exp\left[-\left(\frac{1}{W^2}-\frac{ik}{2F_0}\right)r^2\right] \quad \text{[Eq. A-23]}$$

where

$$W=\frac{2F_0}{kW_0}. \quad \text{[Eq. A-24]}$$

The results show that even relatively modest diversions of power from the $TEM_{0,0}$ mode can have significant impacts on the peak intensity at the target of a focused

beam. Figure A-1 and Figure A-2 give an arbitrary, illustrative example. Figure A-1 shows the two-dimensional intensity profile when all the beam's power is in the $TEM_{0,0}$ mode, and Figure A-2 gives the intensity profile when 10 percent of the power is in the $TEM_{2,2}$ mode. The peak intensity is only 60 percent as great in the second case as in the first.

Figure A-1. Intensity Profile of $TEM_{0,0}$ Beam

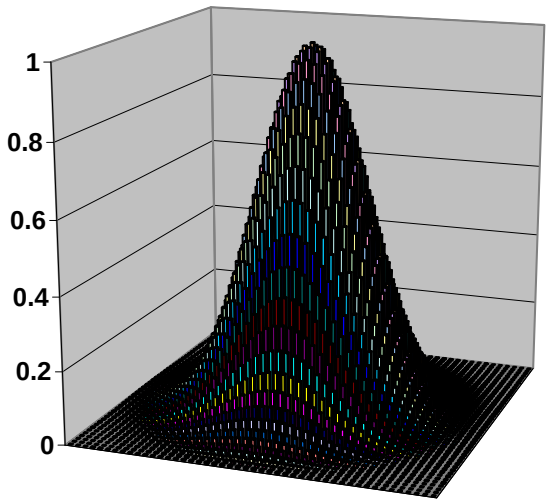

Figure A-2. Intensity Profile of Beam with 90 Percent of Power in $TEM_{0,0}$,10% in $TEM_{2,2}$

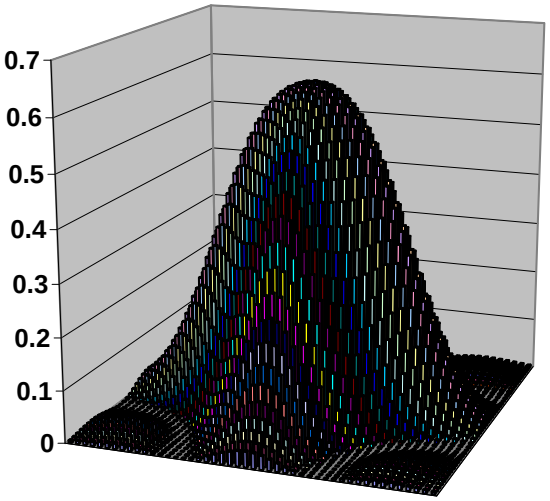

The fact that modest departures from a pure Gaussian$TEM_{0,0}$ mode can have significant effects should not be surprising, since the $TEM_{0,0}$ mode is a highly

idealized case. Pampaloni and Enderlein [5] have shown that it is the beam with simultaneously minimal divergence and minimum transverse extension.

Initial conditions other than Gaussian beams have been considered in the laser propagation literature. For example, the American Physical Society (APS) study of boost-phase intercept systems [6] implicitly assumes that $U_0(x_1, x_2)$ is a truncated spherical wave. This assumption also underlies some of the work in LMI Report PA304T3.

We will continue our work assuming, as do many studies, that all the beam's energy is in the $TEM_{0,0}$ mode. But we note that achieving this in an actual device is a challenge.

Effect of Diffraction on a $TEM_{0,0}$ Beam

Figure A-1 illustrates the effect of diffraction on a $TEM_{0,0}$ Gaussian beam. Specifically, as shown in the mathematical note, at the focal plane $x_3 = F$, this beam's intensity is given by

$$I = \frac{P_{00}}{\pi w^2} e^{-\frac{r^2}{w^2}} \qquad \text{[Eq. A-25]}$$

where P_{00} is the total power in the beam, and

$$w = \frac{\sqrt{2}F_0}{kW_0} = \frac{1}{\sqrt{2}\pi}\frac{\lambda}{W_0}F_0 . \qquad \text{[Eq. A-26]}$$

Relating the reference length W_0 of the Gaussian beam to the diameter D of the mirror that launched the truncated spherical beam considered by the APS so as to make the on-axis intensity the same in both cases implies

$$W_0 = \frac{D}{\sqrt{8}} \qquad \text{[Eq. A-27]}$$

and leads to the comparison between intensity patterns of the Gaussian and truncated spherical beams shown in Figure A-3. The relatively close agreement suggests that considering Gaussian TEM_{00} beams for damage effects of high-power laser beams is not likely to lead to different conclusions from considering truncated spherical beams, as was done in LMI Report PA304T3.

Figure A-3. Intensity Comparison

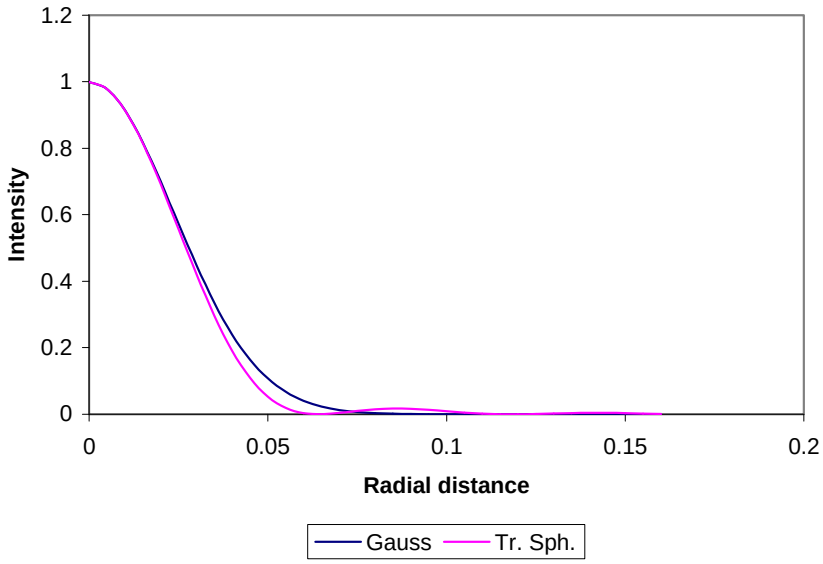

TURBULENCE

To account for the effects of atmospheric turbulence, we return to Equation A-14 written in the form

$$U(\vec{x}) = \frac{-k^2}{4\pi}\iiint_{R^+} G(\vec{x},\vec{y})\chi(\vec{y})U(\vec{y})dv_y + U_f(\vec{x}) \qquad \text{[Eq. A-28]}$$

where U_f is the free-space solution given by the U of Equation A-23.

It will prove convenient to write Equation A-28 in the form

$$U(\vec{x}) = H[U] + U_f(\vec{x}) \qquad \text{[Eq. A-29]}$$

where the operator H is defined by

$$\mathrm{H[U(\vec{x})]} \equiv \frac{-\mathrm{k}^2}{4\pi}\iiint_{\mathrm{R}^+} \mathrm{G}(\vec{x},\vec{y})\chi(\vec{y})\mathrm{U}(\vec{y})\mathrm{dv}_y \,. \qquad \text{[Eq. A-30]}$$

Equation A-28 is a second-kind Fredholm equation, a member of a widely studied class. In particular, arguments such as those given by Oden [7] show that, provided the largest value of $|\chi|$ in the beam region is sufficiently small, the sequence of successive approximations

$$\begin{aligned} u_0(\vec{x}) &= U_f(\vec{x}), \\ u_{n+1}(\vec{x}) &= H[u_n] + U_f(\vec{x}) \end{aligned} \qquad \text{[Eq. A-31]}$$

will converge to the unique solution of Equation A-29. This sequence, called the Born sequence, has been used to discuss effects of atmospheric turbulence. The approximation of the solution of Equation A-28 by the j^{th} term in the sequence of Equation A-31 is called the j^{th} Born approximation.

An approximation developed by Rytov and others models $U(\vec{x})$ as

$$U(\vec{x}) = U_f(\vec{x})e^{\psi_1+\psi_2+\ldots} \qquad \text{[Eq. A-32]}$$

where ψ_j is taken to have magnitude $O(\varepsilon^j)$, $\varepsilon = \|H\|$. Substituting the right side of Equation A-32 for U in Equation A-29 and equating terms of orders ε and ε^2 gives

$$\psi_1 = \frac{1}{U_f} H[U_f] \qquad \text{[Eq. A-33]}$$

and

$$\psi_2 = \frac{1}{U_f} H[U_f \psi_1] - \frac{1}{2}\psi_1^2 . \qquad \text{[Eq. A-34]}$$

Results of Prokhorov [8] and others, described by Hufnagel [9], show that ensemble averages of laser beam intensity in the focal plane are approximately Gaussian, with peak (center) intensity $<I>(0, F_0)$ given by[2]

$$<I>(0,F_0) = I0\frac{w_0^2}{\left(w\left[1+0.46D_w(2F_0/kw)\right]^{\frac{3}{5}}\right)^2} \qquad \text{[Eq. A-35]}$$

where I0 is the intensity at the center of the initial beam, where

$$w_0 = \frac{W_0}{\sqrt{2}}, \quad w = \frac{F_0}{kw_0}, \qquad \text{[Eq. A-36]}$$

and where

$$D_w(2F_0/kw) = 9.25k^{\frac{1}{3}}w^{-\frac{5}{3}}\int_{s=0}^{F} C_n^2(h(s))(F_0-s)^{\frac{5}{3}}ds . \qquad \text{[Eq. A-37]}$$

In Equation A-37, s is arc length along the path of the beam's axis, h(s) is the height of the axis, and $C_n^2(h)$ is the refractive index structure function of the turbulent atmosphere, which, as the notation indicates, we assume is a function of height only.

[2] Equation A-35 corrects a typographical error in Equation 35 of LMI report [2].

The beam's radial intensity profile is approximately Gaussian, with e-folding length w_{turb} given by

$$w_{turb} = w\left[1 + 0.46 D_w (2F_0 / kw)\right]^{\frac{3}{5}}. \qquad \text{[Eq. A-38]}$$

Using methods described later in this appendix, we evaluated the path integrals of Equation A-37 numerically to calculate the effects of turbulence on a laser beam. We also used the method in the section on extinction to generate models of the atmospheric extinction coefficient β as a function of h from PcLnWin outputs. Finally, we applied the blooming calculations of Weichel in the way described in the section on blooming to determine effects of blooming. That section also includes an extended discussion of the turbulence-induced variation of beam radius with distance along the axis, which we used to calculate blooming.

EXTINCTION

Our basic source of extinction information was PcLnWin, a graphical interface to the FASCODE atmospheric code provided by Ontar Corporation. PcLnWin is fully documented in such Ontar publications as *PcLnWin Manual, Version 3* (October 1999).

PcLnWin/FASCODE requires certain user inputs, while providing default values for many FASCODE inputs. We used the following inputs:

- *Line file*. Using data provided with PcLnWin, we built a line file covering the wavenumber interval from 7224.491 cm^{-1} to 7983.610 cm^{-1}, roughly ±5 percent from the chemical oxygen iodine wavenumber of 7604.523 cm^{-1}. The file includes N_2, O_2, H_2O, CO_2, O_3, N_2O, CO, and CH_4 molecules.

- *Atmosphere*. We developed results for three of PcLnWin's available atmosphere models: 1976 Standard Atmosphere, and two models assembled by Ontar from various sources to treat the winter atmosphere in mid-latitudes (MLW), and the summer atmosphere in mid-latitudes (MLS).

- *Aerosol*. We chose FASCODE's Rural aerosol. This choice gives 23 km visibility at the surface.

- *Troposphere/stratosphere.* This transition was determined by the atmosphere model used.

From PcLnWin outputs, we obtained transmissivity T on 1-km paths at heights from 0.1 to 15 km above the surface. These data allowed us to tabulate extinction coefficients β at the observed altitudes, as

$$\beta = -\ln(T)\,\mathrm{km}^{-1}.$$

We then obtained extinction coefficients β(h) at an arbitrary altitude h below 15 km by linear interpolation in the logarithms of the tabulated extinction coefficients.

Figure A-4 compares our model of molecular absorption with the one used by Walter and Mani [10].

Figure A-4. Comparing Molecular Absorption

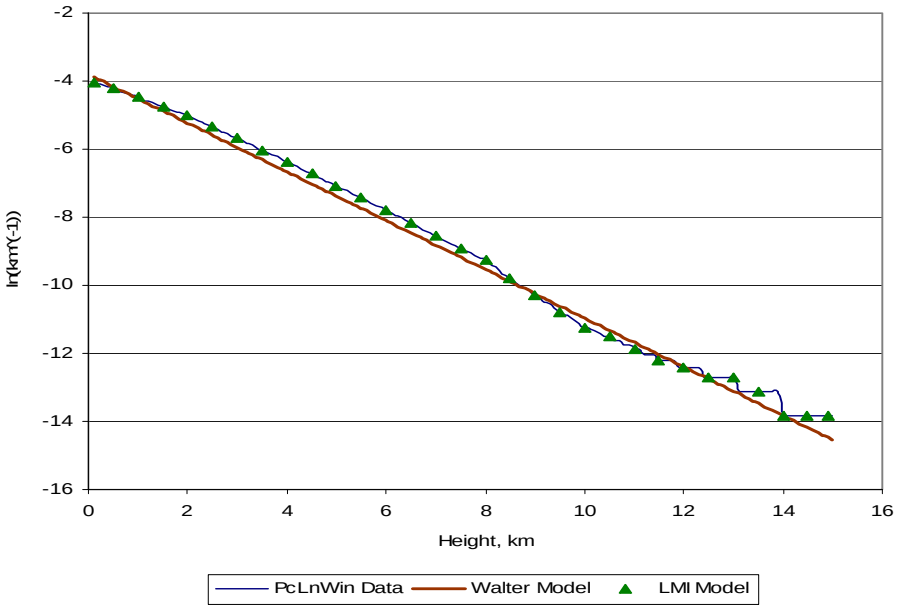

Figure A-5 compares our extinction coefficient with the one used by Walter and Mani [10].

Figure A-5. Extinction Coefficient Model and Data

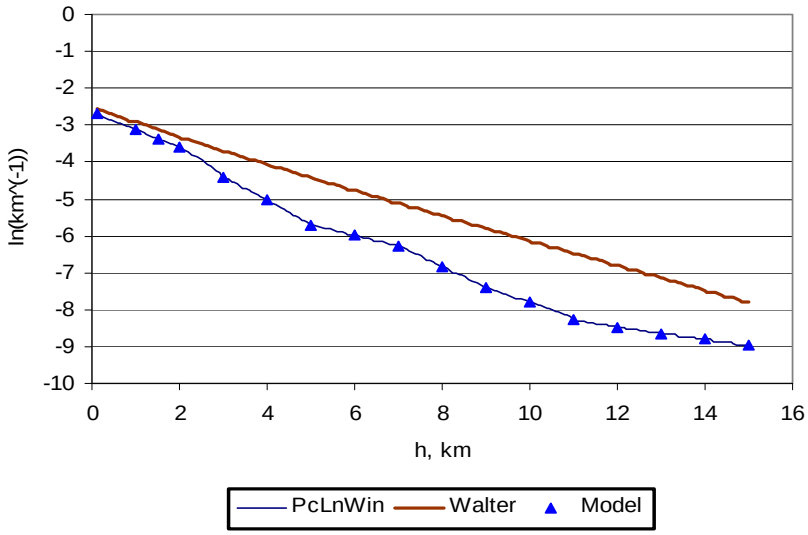

Figures A-4 and A-5 show that, while PcLnWin's molecular absorption agrees closely with Walter's results, PcLnWin's total extinction, and thus by implication aerosol absorption and extinction, are considerably larger for heights of 2 to 5 km than those of the model used by Walter and Mani.

Having extinction coefficients as functions of height allowed us to make numerical calculations of the transmissivity along a path of length L on which height h(s) is given as a function of path length s, as a path integral:

$$T = \exp\left(-\int_0^L \beta(h(s))ds \right).$$

We evaluated such integrals numerically, using the method described below in the section on numerical evaluation of path integrals.

BLOOMING

The beam heats the air through which it passes, decreasing refractive index unevenly and distorting the beam. This effect, called "blooming," reduces fluence on the target. Here we consider this effect.

Citing an article by Weichel [11], the APS report [6] on propagation of high-power laser beams says that, for a Gaussian beam having an e-folding radius a(z) where z is path length, the ratio of the intensity at the target with blooming to that without blooming is

$$\frac{I(Bloom)}{I(NoBloom)} = \frac{1}{1+(B_0 I_B)^2} \qquad \text{[Eq. A-39]}$$

where

$$B_0 = -\frac{dn_0}{dT}\frac{\alpha_0 P L^2}{4\pi\rho_0 w_0 a_0^3} \qquad \text{[Eq. A-40]}$$

and

$$I_B = \frac{2}{L^2}\int_{z=0}^{L}\frac{a_0}{a(z)}\left[\int_{z'=0}^{z}\frac{a_0^2 w_0 \alpha(z')T_0}{a^2(z')w(z')\alpha_0 T(z')}dz'\right]dz \qquad \text{.[Eq. A-41]}$$

In Equations A-40 and A-41, $\alpha(z)$ denotes the part of the atmospheric extinction coefficient that puts power into the air through which the beam passes, w(z) the effective wind velocity coming from the motion of the beam relative to the (possibly moving) atmosphere, T(z) the temperature, and a(z) the beam radius, all varying with distance z along the path. The subscript 0 on any of these denotes the corresponding value at z = 0.

We used the model of atmospheric extinction described above in the section on extinction for the normalized extinction coefficient $\frac{\alpha(z)}{\alpha_0}$. The following subsections explain how we evaluated normalized beam radius $\frac{a(z)}{a_0}$ and wind normalized wind profile $\frac{w(z)}{w_0}$.

Beam Radius

For the variation of beam radius a(z), we considered the variation from the mirror radius at z = 0 to the radius of the turbulence-broadened, focused spot at z = L. By "turbulence-broadened, focused spot" we mean what Fante [12] calls the "short-term beam spread" for the focused beam. As Fante explains, long-scale turbulence causes the beam to wander, while short-scale turbulence spreads it out. Thus the target receives a broadened, wandering spot (Figure A-6).

Figure A-6. Broadened, Wandering Spot

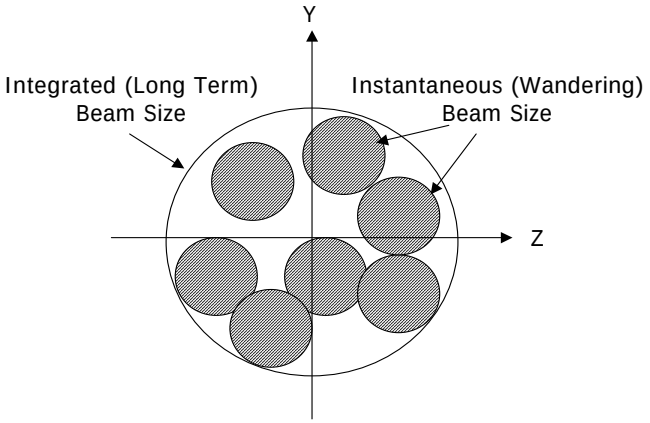

Source: After Fante [12], footnote 5.

We assume that the heating that causes blooming is influenced by the broadening, but not by the wandering.

Fante [12] gives means of calculating the mean e-folding radius of the broadened spot, ρ_s, as a fraction $\mu(\rho_0)w_{turb}$, where

$$\rho_0 = \left[1.46k^2 L \int_0^1 C_n^2(\xi L)(1-\xi)^{\frac{5}{3}} \right]^{-\frac{3}{5}}. \qquad \text{[Eq. A-42]}$$

When ρ_0 is either much less than or much greater than the initial beam radius, Fante [12] provides analytic expressions for $\mu(\rho_0)$. As shown by Figure A-7, neither of those conditions is likely to be met for mirrors of the size likely to be used in laser weapons for tactical aircraft, except perhaps at very low altitudes and extreme ranges.[3] Rather, in the situations ALIRT is intended to treat, ρ_0 is roughly the same size as the initial beam radius.

Figure A-7. Variation of ρ_0

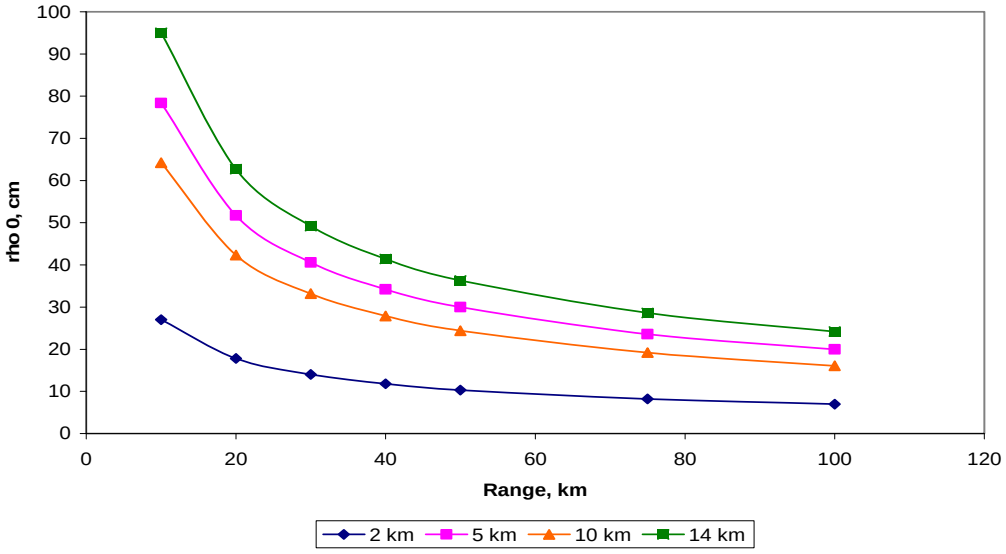

Fante [12] provides numerical means of calculating ρ_s when ρ_0 is roughly the same size as the initial beam radius. We have incorporated Fante's method for this in ALIRT, by making a numerical model of Figure 3 of [12].

Figure A-8 compares the mean radius of the broadened, wandering beam with that of the broadened beam without effects of wandering, and with the radius of the Gaussian beam propagating from the laser in free space, for a horizontal shot from a laser weapon at 7 km height.

[3] Figure A-7 also shows the non-monotone variation of C_n^2 with height: high-altitude winds and corresponding turbulence give C_n^2 a maximum at around 10 km height.

Figure A-8. Comparison of Beam Radii, Horizontal Shot at 7 km Height

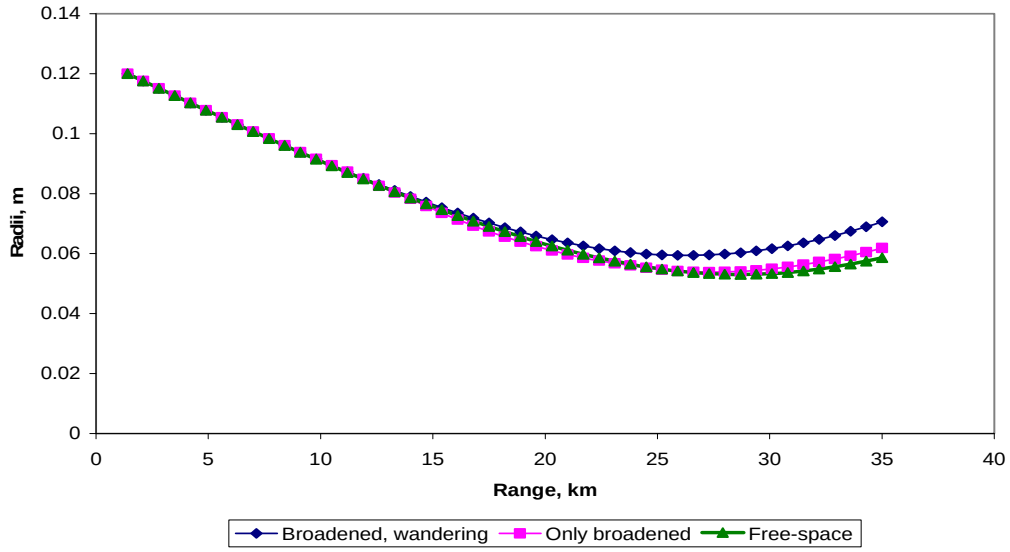

The figure indicates that broadening does not cause substantial departures of short-time average beam radius from the free-space case at heights of several kilometers and ranges of some tens of kilometers, though wandering does cause the long-time average beam radius to be significantly larger than that of the free-space beam in such cases.

One would expect greater impact of turbulence when beams propagate through regions of greater turbulence intensity, and this is borne out by calculations. Figure A-9 shows the same comparison as Figure A-8, but for a horizontal shot at a height of 2 km. The figure indicates that turbulence-induced broadening and wandering are significant for shots at lower altitudes.

Figure A-9.Comparison of Radii, Horizontal Shot at 2 km Height

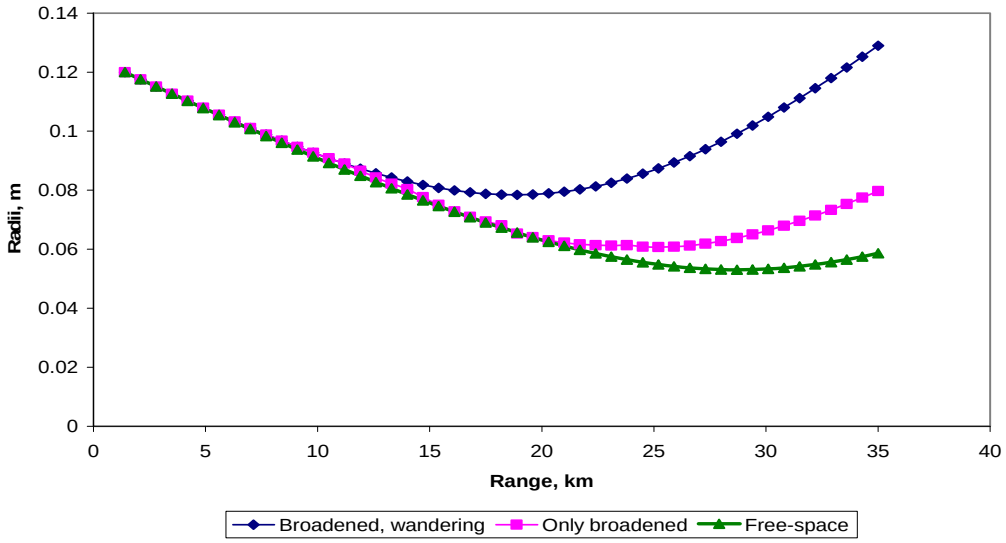

To evaluate the iterated integral of Equation A-41 with a single integral, we note that

$$\int_{z=0}^{L} \frac{a_0}{a(z)} \left[\int_{z'=0}^{z} \frac{a_0^2 w_0 \alpha(z') T_0}{a^2(z') w(z') \alpha_0 T(z')} dz' \right] dz = \int_{z'=0}^{L} \frac{a_0^2 w_0 \alpha(z') T_0}{a^2(z') w(z') \alpha_0 T(z')} \left[\int_{z=L}^{z''} \frac{a_0}{a(z)} dz \right] dz' \qquad \text{[Eq. A-43]}$$

and that the integral with respect to z can be evaluated numerically, using values of the variation of the broadened beam along the beam axis:

$$\int_{z=L}^{z''} \frac{a_0}{a(z)} dz \equiv g(z') \qquad \text{[Eq. A-44]}$$

With the g(z′) determined in Equation A-44, and using values of $T_0/T(z')$ from the 1976 Standard Atmosphere, we evaluated I_B numerically as

$$I_B = \int_{z'=0}^{L} \frac{a_0^2 w_0 \alpha(z') T_0}{a^2(z') w(z') \alpha_0 T(z')} g(z')\, dz'. \qquad \text{[Eq. A-45]}$$

Wind Profile

We needed to develop a wind profile w(z) that is realistic, and for which the integral of Equation A-45 converges, and for which Equation D.29 of APS [6] will apply. That equation, specifically,

$$\rho c_p w \frac{\partial T}{\partial x} = \alpha I, \qquad \text{[Eq. A-46]}$$

is the starting point of the blooming analysis of that reference.

For air-to-air engagements (except for shots made flying directly toward the target or away from it) the wind relative to the beam will be large along the entire path, Equation A-45 will apply, and the integral will certainly converge.

But for a stationary target on the ground, it will not do simply to take the velocity profile generated by the motion of the beam from aircraft to a fixed ground target. That wind profile may fall linearly to zero at the target, and the integral of Equation A-38 would not converge.

It is, however, possible that typical winds would be large enough for Equation A-45 to apply. If so, then a simple profile w(z) that began with a speed like that of the weapon-bearing aircraft at z = 0, and fell to a typical surface wind speed at z = L, could be used.

We began our consideration of wind profile with the equation

$$\frac{\partial T}{\partial t} + \vec{q} \cdot \nabla T = \frac{k}{\rho c_p} \nabla^2 T + \frac{1}{\rho c_p} Q . \qquad \text{[Eq. A-47]}$$

expressing conservation of energy in an isobaric motion of a fluid with constant specific heat at constant pressure c_p and thermal conductivity k, neglecting viscous dissipation. Equation A-46 is written for an inertial frame moving with the beam *locally*. In Equation A-46, $\vec{q}$ is fluid velocity in cm/sec, T is temperature in ^oK, Q denotes rate of heat addition in watts/cm^3, k is thermal conductivity in watts/(cm ^oK), and ρ is density in g/cm^3.

Introducing non-dimensional variables $\hat{T}, \hat{\vec{q}}, \hat{\vec{x}}$ and $\hat{t}$ with the definitions

$$\begin{aligned} \hat{t} &\equiv \frac{kt}{\rho c_p d^2} \\ \hat{\vec{q}} &\equiv \vec{q} / w \\ \hat{\vec{x}} &\equiv \vec{x} / d \\ \hat{T} &\equiv T / T_{ref} \end{aligned} \qquad \text{[Eq. A-48]}$$

where $\vec{x}$ is position coordinate, w is fluid velocity relative to the beam, and d is beam diameter, brings Equation A-46 to

$$\frac{k}{w\rho c_p d} \frac{\partial T}{\partial t} + \vec{q} \cdot \nabla T = \frac{k}{w\rho c_p d} \nabla^2 T + \frac{w}{d T_{ref}} Q . \qquad \text{[Eq. A-49]}$$

In Equation A-49, we have suppressed the ^ symbols for clarity. Equation A-49 shows that temperature changes will satisfy

$$\vec{q} \cdot \nabla T = \frac{w}{d T_{ref}} Q \qquad \text{[Eq. A-50]}$$

provided that $\frac{k}{w\rho c_p d} << 1$, or, equivalently, that $w >> \frac{k}{\rho c_p d}$. For a representative case, $k = 2.55 \times 1A\text{-}^4$ joule/(sec cm ^oK), $\rho = 1.225 \times 10^{-3}$ g/cm^3, c_p = 1 joule/(g ^oK), and the condition that Equation A-49 governs temperature changes, and w >> 0.01 cm/sec.

This condition is likely to be met by ordinary wind, even if the beam is fixed in space, as it would be on a stationary target on the ground.

With this result in mind, we developed the profile of wind relative to the beam in this way: If $\vec{V}_P$ and $\vec{V}_T$ denote, respectively, the velocity vectors of platform and target, and if $\vec{W}$ denotes the wind velocity, then at a point on the beam located a fraction ς of the distance from platform to target, the beam will have velocity

$$\vec{V}(\varsigma) = \vec{V}_P + \varsigma(\vec{V}_T - \vec{V}_P) + \vec{W}(\varsigma)). \qquad \text{[Eq. A-51]}$$

The magnitude V_{perp} of the velocity perpendicular to the beam will be given by the magnitude of the cross product of a unit vector parallel to the beam, and the beam's velocity $\vec{V}$. We evaluated that cross product, arbitrarily choosing the components of $\vec{W}$ to be a constant 2 m/s in each of three perpendicular directions, to obtain w(z).

In addition to parameters determined in evaluating I_B, evaluating B_0 required only a value for $\frac{1}{\rho_0}\frac{dn_0}{dT}$. We used the value -1×10^{-3} cm^3/(g ^{o}K) given in the APS report cited above.

BEAM-TARGET INTERACTION

The laser beam will not necessarily strike the target's surface perpendicularly, and the target surface will not necessarily be a plane. Here we consider these effects.

For perpendicular incidence, the target experiences the intensity in the focal plane $x_3 = F_0$. Otherwise, we must consider variations in x_3 as well as in x_1 and x_2, when x_3 is close to F_0.

For a TEM_{00} beam, the most sensitive variation is in the term

$$\exp\left[-\frac{k^2r^2}{x_3^2}\left(\frac{1}{\frac{1}{W_0^2}+\frac{ik}{2}\Delta}+\frac{1}{\frac{1}{W_0^2}-\frac{ik}{2}\Delta}\right)\right] = \exp\left[\frac{-2k^2r^2W_0^2}{x_3^2(1+k^2W_0^4\Delta^2/4)}\right] \qquad \text{[Eq. A-52]}$$

where $\Delta \equiv 1/F_0 - 1/x_3$ (this follows from Equation A-67 in the mathematical note).

Now, the spot size will limit the variation of x_3 to a few centimeters. Accordingly, the term $\frac{2k^2r^2W_0^2}{x_3^2}$ will vary from $\frac{2k^2r^2W_0^2}{F_0^2}$ by an amount of $O(10^{12}\times10^{-4}\times10^{-2}\times10^{-8}\times10^{-5})$, which will cause negligible change in the quantity of Equation A-52 . Similar considerations show that the term

$k^2 W_0^2 \Delta^2 / 4$ will depart negligibly from 1, while x_3 ranges over the illuminated spot.

Consequently, over the part of the target surface illuminated by the beam, the Poynting vector will be

$$\vec{P} = \frac{P_{00}}{\pi w^2} e^{-\frac{r^2}{w^2}} \vec{e}_3 \qquad \text{[Eq. A-53]}$$

where w is given by the w_{turb} of Equation A-38 and $\vec{e}_3$ is a unit vector in the beam-propagation direction.

Let us first consider a plane target surface. Without loss of generality, for a TEM_{00} beam, we may take the direction of x_1 to be perpendicular to the plane defined by the beam-propagation direction and the normal to the surface. If, then, y_1 is a coordinate in the plane of the target, parallel to x_1, and y_2 is a coordinate in the plane of the target, perpendicular to y_1, in the target plane, the intensity will be

$$I_{target} = \cos\theta \frac{P}{\pi w^2} \exp\left[\frac{y_1^2 + y_2^2 \cos^2\theta}{w^2}\right] \qquad \text{[Eq. A-54]}$$

where θ is the angle between the normal to the surface and the beam-propagation direction. Curves of constant intensity will be ellipses, and the peak intensity experienced by the target will be reduced by the factor $\cos\theta$. Figure A-10 compares 1 kw/cm^2 contours at normal incidence (circle) and at 60^o incidence (ellipse).

Figure A-10. Comparison of Constant-Intensity Contours

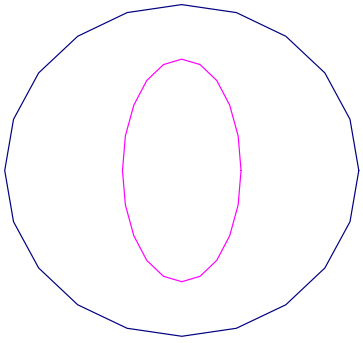

If the target surface is not a plane, but has a continuously turning tangent over the part illuminated by the beam, then it may be parameterized by

$$y_3 = Y_3(y_1, y_2) \equiv \frac{(y_1 \cos\gamma + y_2 \sin\gamma)^2}{R_1} + \frac{(-y_1 \sin\gamma + y_2 \cos\gamma)^2}{R_2} \qquad \text{[Eq. A-55]}$$

where y_3 is a coordinate measured perpendicular to the plane of y_1 and y_2, where R_1 and R_2 are the principal radii of curvature, and where γ is the angle between the direction of y_1 and the direction of the plane of principal curvature R_1.

With Equation A-54 and Equation A-55, one may write an expression for the luminous flux into the surface at the point (y_1, y_2, $Y_3(y_1, y_2)$). The result will differ from Equation A-52 for constant θ by a multiplicative factor whose difference from unity is bounded in magnitude by the largest value of $\sqrt{y_1^2 + y_2^2}$ in the illuminated spot, divided by the smaller of R_1 and R_2, and multiplied by the largest value of $\sin\theta$.

Since $\sqrt{y_1^2 + y_2^2}$ is typically not larger than about 10 cm in the spot, and for reasonable angles of incidence $\sin\theta$ is $O(10^{-1})$, the multiplicative factor will differ from unity by $O(10^{-2})$, and curvature will be negligible, if the smaller principal radius of curvature is O(1 m).

It seems reasonable to assume that that will be the case, when the target is a fighter or bomber aircraft. Accordingly, we will not consider curvature further here. For such targets as air-to-air, ground-to-air, or ground-to-ground tactical missiles, however, curvature effects may be significant and should be considered.

NUMERICAL EVALUATION OF PATH INTEGRALS

We evaluated path integrals such as the one in Equation A-37 numerically. To do so, we needed to compute the path taken by the laser's output through the atmosphere undisturbed by turbulence.

Effects of oxygen and nitrogen molecules dominate the atmosphere's refractive index. Following the expression for n given by Thomas and Duncan [13], we used

$$n = 0.079P / T \qquad \text{[Eq. A-56]}$$

where P is pressure in atmospheres and T is temperature in ^{o}K.

For MLS and MLW atmospheres, we used analytic models of PcLnWin refractive index outputs. Calculation of the refracted ray requires derivatives of refractive index variation with height, so a continuously differentiable model is desirable. We made the models by linear interpolation in the divided differences of refractive index parameter, and integrated the resulting piecewise linear, continuous function with an added, adjustable constant of integration to obtain a continuously differentiable model of refractive index. Figure A-11 shows the comparison between our model of the refractive index parameter $1e^6(n - 1)$, where n is refractive index, and the PcLnWin data for MLS.

Figure A-11. Verification of MLS Refractive Index Model

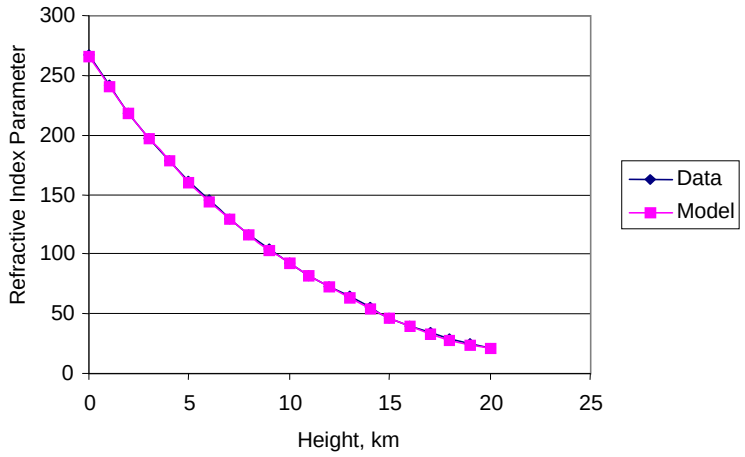

Figure A-12 shows the comparison between divided differences of the refractive index parameter, and the derivative of our model of the refractive index parameter for MLS. The tropopause is clearly noticeable.

Figure A-12. Verification of Derivative of MLS Refractive Index Model

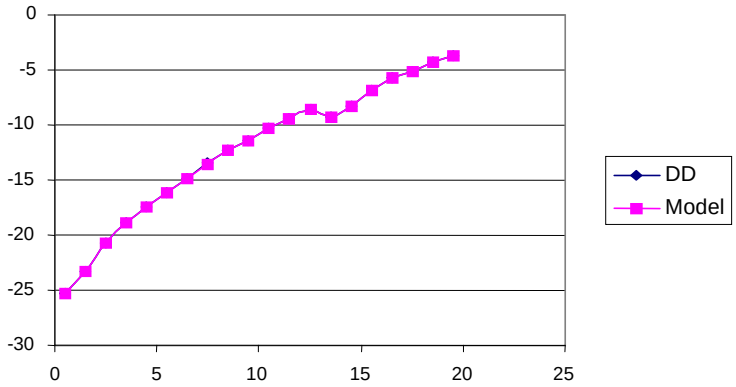

The refractive index variation of Thomas and Duncan [13] is not large; it is about 0.0003 near the surface. Also, tactical laser weapons will be used at medium ranges, generally no greater than 100–200 km. It is possible that using straight paths would not greatly distort integrals like that of Equation A-37.

Two considerations militate against neglecting refraction, however. First, refraction is noticeable at extreme ranges and low weapon altitudes. Second, C_n^2 varies sharply with height, so path variations may have significant effects. For example, C_n^2 differs by more than 10 percent on substantial parts of the two paths shown in Figure A-13 (the great difference between the scales of the ordinate and abscissa of the figure distorts geometry).

Figure A-13. Refracted and Straight Paths

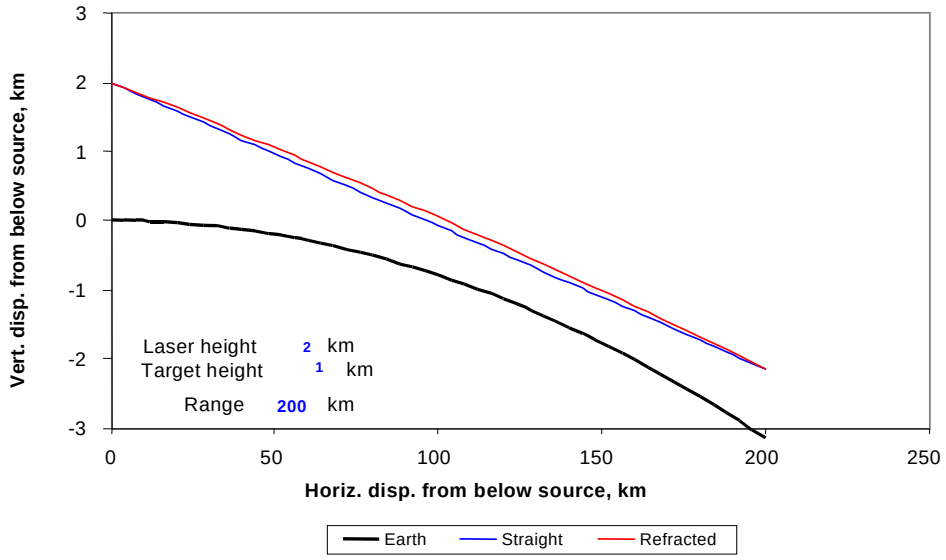

Accordingly, we determined refracted paths numerically. We did so by integrating the beam equation (from Born and Wolf [14])

$$\frac{d}{ds}(n\underline{\tau}) = \nabla n$$

and the relation

$$\frac{d\underline{r}}{ds} = \underline{\tau}$$

between the vector $\underline{r}(s)$, which gives the position of the point on the ray at path length s and the unit tangent vector $\underline{\tau}$ numerically, using the difference scheme

$$n_{i+1}\underline{\tau}_{i+1} = n_i\underline{\tau}_i + (\nabla n)_i \Delta s$$
$$\underline{r}_{i+1} = \underline{\tau}_i \Delta s$$

suggested by Berton [15].

We started the refracted path with the user-specified altitude and elevation angle, which gave us $\underline{r}(0)$ and $\underline{\tau}(0)$, respectively. Please note that starting with a specified value of $\underline{\tau}$ means that we start the ray in the direction at which an observer looking with the laser radiation would see the target, not the direction of the straight line to the target and not necessarily the direction at which observer looking with radiation of a different wavelength would see the target.

Numerical solution of the beam and tangent equations gave us the array $h(s_i)$ specifying beam height at path length s_i. This allowed us to evaluate the integrands of path integrals like the one in Equation A-37, which have the form F(s, h(s)), and then to approximate the integral numerically by the trapezoidal rule.

MATHEMATICAL NOTE

To evaluate

$$I_n \equiv \int_{-\infty}^{\infty} e^{\frac{ik}{2x_3}(x-y)^2} e^{-\left(\frac{1}{W_0^2}+\frac{ik}{2F_0}\right)y^2} H_n\left(\frac{\sqrt{2}y}{W_0}\right) dy\,, \qquad \text{[Eq. A-57]}$$

we use the contour integral representation for Hermite polynomials,

$$H_n(x) = \frac{n!}{2\pi i}\oint_c \frac{1}{z^{n+1}} e^{2xz-z^2}\,, \qquad \text{[Eq. A-58]}$$

where the contour C is a circle enclosing z = 0, traversed counter-clockwise (Abramowitz and Stegun [16], Equation 22.10.9). The representation generates $H_n(x)$ for arbitrary complex x.

Substituting the contour integral in Equation A-58 for H_n in Equation A-57 and exchanging the order of integration gives

$$I_n = \frac{n!}{2\pi i}\oint_c \frac{e^{-z^2}}{z^{n+1}} \int_{-\infty}^{\infty} e^{\frac{ik}{2x_3}(x-y)^2 - \alpha y^2 + 2\frac{\sqrt{2}}{W_0}yz}\, dy\, dz \qquad \text{[Eq. A-59]}$$

where

$$\alpha \equiv \frac{1}{W_0^2} + \frac{ik}{2F_0}\,. \qquad \text{[Eq. A-60]}$$

The inner integral of Equation A-59 is readily evaluated by completing the square. When this is done, we find, after some manipulation, that

$$I_n = \frac{\sqrt{\pi} e^{\frac{ikx^2}{2x_3}+\frac{a^2}{4}} (1-b^2/4)^{\frac{n}{2}}}{\sqrt{\alpha - \frac{ik}{2x_3}}} H_n\left(\frac{ab}{4\sqrt{1-b^2/4}}\right) \qquad \text{[Eq. A-61]}$$

where

$$a = \frac{ikx}{x_3\sqrt{\alpha - \frac{ik}{2x_3}}}; \quad b = -\frac{2\sqrt{2}}{W_0\sqrt{\alpha - \frac{ik}{2x_3}}}. \qquad \text{[Eq. A-62]}$$

Considerable further manipulation shows that

$$1 - \frac{b^2}{4} = -\frac{1 - \frac{ikW_0^2}{2}\Delta}{1 + \frac{ikW_0^2}{2}\Delta} \qquad \text{[Eq. A-63]}$$

where

$$\Delta \equiv \frac{1}{F_0} - \frac{1}{x_3} \qquad \text{[Eq. A-64]}$$

and, consequently, that

$$\left[1 - \frac{b^2}{4}\right]^{\frac{n}{2}} = e^{i\frac{n}{2}\left(\pi - \arctan\left(\frac{k^2W_0^2\Delta^2}{4}\right)\right)}. \qquad \text{[Eq. A-65]}$$

Also,

$$\frac{ab}{4\sqrt{1 - b^2/4}} = \frac{kW_0 x}{\sqrt{2}x_3\left[1 + \frac{k^2W_0^4}{4}\Delta^2\right]^{\frac{1}{2}}} \qquad \text{[Eq. A-66]}$$

so that the argument of the Hermite polynomial is a real number.

For the particular case n = 0,

$$I_0 = \sqrt{\frac{\pi}{\alpha - \frac{ik}{2x_3}}} e^{\frac{ikx^2}{2x_3} - \frac{kx^2}{4(\alpha - ik/2x_3)}}. \qquad \text{[Eq. A-67]}$$

If the integral is evaluated in the focal plane $x_3 = F_0$, then $\Delta = 0$, and

$$\left[1 - \frac{b^2}{4}\right] = -1; \quad \left[1 - \frac{b^2}{4}\right]^{\frac{n}{2}} = i^n, \qquad \text{[Eq. A-68]}$$

$$\frac{ab}{4\sqrt{1-b^2/4}} = \frac{kW_0 x}{\sqrt{2}F_0}, \qquad \text{[Eq. A-69]}$$

and

$$I_n = \sqrt{\pi} e^{\frac{ikx^2}{2F_0} - \frac{k^2 x^2 W_0^2}{4F_0^2}} W_0 i^n H_n\left(\frac{kW_0 x}{\sqrt{2}F_0}\right). \qquad \text{[Eq. A-70]}$$

Using the result of Equation A-70 to evaluate the integral expression of Equation A-21 for $U(x_1, x_2, F_0)$ when $U_0(x_1, x_2)$ is given by Equation A-22 leads, after straightforward manipulation, to

$$U(x_1, x_2, F_0) = \frac{-i}{W} \sum\sum e^{i\phi_{mn}} i^{m+n} \sqrt{\frac{P_{mn} R_0}{2^{m+n-2} \pi m! n!}} H_m\left(\frac{\sqrt{2}x_1}{W}\right) H_n\left(\frac{\sqrt{2}x_2}{W}\right) \exp\left[-\left(\frac{1}{W^2} - \frac{ik}{2F_0}\right) r^2\right] \qquad \text{[Eq. A-71]}$$

where

$$W \equiv \frac{2F_0}{kW_0}. \qquad \text{[Eq. A-72]}$$

If, finally, the sum in Equation A-71 has just two terms, with $\varphi_{00} = 0$, $\varphi_{22} = \pi$, and a fraction γ of the total power is in the TEM_{22} mode, then the focal plane intensity will satisfy

$$I \propto \left[\left[\sqrt{2(1-\gamma)}\right] - \sqrt{\frac{\gamma}{32}} H_2(x_1/w) H_2(x_2/w)\right]^2 \exp^{-\frac{r^2}{w^2}} \qquad \text{[Eq. A-73]}$$

where

$$w \equiv \frac{W}{\sqrt{2}}. \qquad \text{[Eq. A-74]}$$

REFERENCES

[1] LMI, *Analytic Methods for Tactical Air Warfare: Air Campaign and High-Energy Laser Propagation Analyses*, Report PA304T1, David A. Lee and others, September 2004.

[2] LMI, *2007 Atmospheric Laser and Infrared Transmission Model: Some Considerations for Interactions of High-Power Laser Beams with Targets*, Report PA603T3, David A. Lee, September 2007.

[3] Ontar Corporation, *PcLnWin Manual, Version 3*, October 1999.

[4] Andrews and Ronald L. Phillips, *Laser Beam Propagation through Random Media* (Bellingham, WA: SPIE Optical Engineering Press, 1998).

[5] F. Pampaloni and Jörg Enderlein, "Gaussian, Hermite-Gaussian, and Laguerre-Gaussian Beams: A Primer," arxiv.org/ftp/physics/papers/0419/0410021.pdf, 2004.

[6] American Physical Society, *Report of the American Physical Society Study Group on Boost-Phase Intercept Systems for National Missile Defense*, July 2003.

[7] J.T. Oden, *Applied Functional Analysis* (Englewood Cliffs, NJ: Prentice-Hall, 1979), Example 4.8.6, p. 231.

[8] F.V. Prokhorov, K.S. Bunkin, K.S. Gochelashvily, and V.I. Shishov, "Laser Irradiance in Turbulent Media," *Proceedings of the IEEE*, Vol. 63 (1975), pp. 790–809.

[9] R.E. Hufnagel, "Propagation through Atmospheric Turbulence," Chapter 6 of *The Infrared Handbook*, William L. Wolfe and George Zissis, Editors, Office of Naval Research, Department of the Navy, 1978.

[10] Robert Walter and Siva Mani, *Advanced Tactical Laser (ATL) Power-Aperture Trade Studies*, Laser Engineering and Technology Support (LETS), Schafer Corp., Task Order 0008, Contract F29601-98-D-0036, December 31, 2002.

[11] Hugo Weichel, *Laser Beam Propagation in the Atmosphere*, Volume TT 3 (Bellingham, WA: SPIE Optical Engineering Press, 1990).

[12] R.L. Fante, "Electromagnetic Beam Propagation in Turbulent Media," *Proceedings of the IEEE*, Vol. 63, No. 12 (December 1976), pp. 1,669–1,692.

[13] M.E. Thomas and D.D. Duncan, “Atmospheric Transmission,” Chapter 1 of *Atmospheric Propagation of Radiation*, in Volume 2 of *The Infrared and Electro-Optical Systems Handbook,* F. G. Smith, Editor (copublished by The Infrared Information Analysis Center of the Environmental Institute of Michigan and SPIE Optical Engineering Press, Bellingham, WA).

[14] Max Born and Emil Wolf, *Principles of Optics* (Oxford: Pergamon Press, 1980).

[15] Roland P.H. Berton, “Variational Calculation of Three-Dimensional Atmospheric Refraction: Part I, Description and Validation of the Method,” *Journal of Optics A: Pure and Applied Optics,* August 2006, pp. 817–830.

[16] M. Abramowitz and Irene A. Stegun, Editors, *Handbook of Mathematical Functions*, Eighth Dover Printing (New York: Dover, December 1972).

REPORT DOCUMENTATION PAGE

Form Approved
OMB No. 0704-0188

1. REPORT DATE *(MM-YYYY)*	2. REPORT TYPE	3. DATES COVERED *(From - To)*
01-2009	Final	9/28/07 – 1/30/09

4. TITLE AND SUBTITLE
Atmospheric Laser And Infrared Transmission Model

5a. CONTRACT NUMBER
W91QZ-07-F-0076

5b. GRANT NUMBER

5c. PROGRAM ELEMENT NUMBER

6. AUTHOR(S)
Hemm, Jr., Robert V.
Lee, David A.

5d. PROJECT NUMBER

5e. TASK NUMBER

5f. WORK UNIT NUMBER

7. PERFORMING ORGANIZATION NAME(S) AND ADDRESS(ES)

LMI
2000 Corporate Ridge
McLean, VA 22102-7805

8. PERFORMING ORGANIZATION REPORT NUMBER
PA702T2

9. SPONSORING / MONITORING AGENCY NAME(S) AND ADDRESS(ES)
Mr. Frank Lewis
OSD/Program Analysis and Evaluation - TACAIR
Pentagon, Rm 2C281
washington, DC 20301-1800

10. SPONSOR/MONITOR'S ACRONYM(S)

11. SPONSOR/MONITOR'S REPORT NUMBER(S)

12. DISTRIBUTION / AVAILABILITY STATEMENT

A Approved for public release; distribution is unlimited

13. SUPPLEMENTARY NOTES

14. ABSTRACT

This report documents the Atmospheric Laser and Infrared Transmission (ALIRT) model developed by LMI for OSD/PA&E TACAIR. The report includes a description of the model and its structure, a user's guide, and an extended mathematical description of the model physics. ALIRT models high energy laser propagation from moving or stationary platforms to moving or stationary targets. Transmission effects include diffraction plus atmospheric refraction, diffraction, scatter, absorption, and thermal blooming. The model also considers target incidence. The current versions of ALIRT model 1.315 micron iodine and 1.060 micron solid state laser wavelengths. Addition of other wavelengths is straightforward. The model is coded in Microsoft Excel Visual Basic and runs on a personal computer.

15. SUBJECT TERMS
airborne laser, infrared tracking model, air-to-air combat, high energy laser, Atmospheric Laser and Infrared Transmission, ALIRT, solid state laser, iodine laser

16. SECURITY CLASSIFICATION OF:			17. LIMITATION OF ABSTRACT	18. NUMBER OF PAGES	19a. NAME OF RESPONSIBLE PERSON
a. REPORT	b. ABSTRACT	c. THIS PAGE	Unclassified Unlimited	44	Nancy E. Handy
UNCLASSIFIED	UNCLASSIFIED	UNCLASSIFIED			19b. TELEPHONE NUMBER *(include area code)* 703-917-7249